Journal of Inorganic Biochemistry 135 (2014) 10–19

Contents lists available at ScienceDirect

Journal of Inorganic Biochemistry

journal homepage: www.elsevier.com/locate/jinorgbio

Mechanism of reaction of chlorite with mammalian heme peroxidases

Christa Jakopitsch [a], Katharina F. Pirker [a], Jörg Flemmig [b,c], Stefan Hofbauer [a], Denise Schlorke [b], Paul G. Furtmüller [a], Jürgen Arnhold [b,c], Christian Obinger [a,*]

[a] Department of Chemistry, Division of Biochemistry, BOKU — University of Natural Resources and Life Sciences, Muthgasse 18, A-1190 Vienna, Austria
[b] Institute for Medical Physics and Biophysics, Medical Faculty, University of Leipzig, Härtelstr 16-18, D-04107 Leipzig, Germany
[c] Translational Centre for Regenerative Medicine, University of Leipzig, Philipp-Rosenthal-Strasse 55, D-04103 Leipzig, Germany

ARTICLE INFO

Article history:
Received 12 December 2013
Received in revised form 19 February 2014
Accepted 19 February 2014
Available online 28 February 2014

Keywords:
Myeloperoxidase
Lactoperoxidase
Chlorite
Hypochlorous acid
Chlorine dioxide
Oxoferin

ABSTRACT

This study demonstrates that heme peroxidases from different superfamilies react differently with chlorite. In contrast to plant peroxidases, like horseradish peroxidase (HRP), the mammalian counterparts myeloperoxidase (MPO) and lactoperoxidase (LPO) are rapidly and irreversibly inactivated by chlorite in the micromolar concentration range. Chlorite acts as efficient one-electron donor for Compound I and Compound II of MPO and LPO and reacts with the corresponding ferric resting states in a biphasic manner. The first (rapid) phase is shown to correspond to the formation of a MPO-chlorite high-spin complex, whereas during the second (slower) phase degradation of the prosthetic group was observed. Cyanide, chloride and hydrogen peroxide can block or delay heme bleaching. In contrast to HRP, the MPO/chlorite system does not mediate chlorination of target molecules. Irreversible inactivation is shown to include heme degradation, iron release and decrease in thermal stability. Differences between mammalian peroxidases and HRP are discussed with respect to differences in active site architecture and heme modification.

1. Introduction

Chlorite ($^{-}OClO$) reacts with a variety of different heme containing enzymes. For example, it was shown to induce the formation of methemoglobin [1] and might act as hydroxylating agent in cytochrome P450 [2]. However, detailed mechanistic studies are only available for two classes of heme enzymes, namely chlorite dismutases and peroxidases. Chlorite dismutases are found in bacteria and archaea [3,4] and convert chlorite to chloride (Cl^{-}) and dioxygen (O_2) with hypochlorous acid (HOCl) as proposed reaction intermediate [5]. During this conversion a covalent O–O bond is formed, a reaction which was so far only observed at photosystem II of oxygenic phototrophic organisms.

Among heme peroxidases, chlorite was shown to be utilized by cytochrome *c* peroxidase [6], chloroperoxidase [7] and horseradish peroxidase (HRP) [8]. Upon reaction with chlorite the enzymes produced halogenating agents but not O_2. Detailed studies were carried out by Hager and co-workers on HRP [9–11]. Recently, by using sequential-mixing stopped-flow spectroscopy, we have reinvestigated this reaction and could demonstrate that HRP mixed with chlorite follows the whole peroxidase cycle [12]. Chlorite mediates the two-electron oxidation of ferric HRP [Fe(III)…Por] to Compound I [Fe(IV) = O…Por$^{\bullet+}$] thereby releasing hypochlorous acid (Reaction 1). Furthermore, chlorite acts as one-electron reductant of both Compound I and Compound II [Fe(IV) = O…Por] forming chlorine dioxide ($^{\bullet}ClO_2$) (Reactions 2 & 3). The HRP mediated reactions are strongly pH dependent, suggesting that chlorous acid (HOClO) is the reacting species [12]. In addition both reaction products also mediate the two-electron oxidation of ferric HRP to Compound I (Reaction 4 & 5) but cannot serve as electron donors for Compounds I or II.

$$[Fe(III)\ldots Por] + {}^{-}OClO \rightarrow \left[Fe(IV) = O\ldots Por^{\bullet+}\right] + HOCl/{}^{-}OCl, H^{+} \quad \text{(Reaction1)}$$

$$[Fe(IV) = O\ldots Por^{\bullet+}] + {}^{-}OClO \rightarrow [Fe(IV) = O\ldots Por] + {}^{\bullet}ClO_2 \quad \text{(Reaction2)}$$

$$[Fe(IV) = O\ldots Por] + {}^{-}OClO \rightarrow [Fe(III)\ldots Por] + {}^{\bullet}ClO_2 + H_2O \quad \text{(Reaction3)}$$

$$[Fe(III)\ldots Por] + HOCl \rightarrow \left[Fe(IV) = O\ldots Por^{\bullet+}\right] + Cl^{-} \quad \text{(Reaction4)}$$

$$[Fe(III)\ldots Por] + {}^{\bullet}ClO_2 \rightarrow [Fe(IV) = O\ldots Por^{\bullet+}] + {}^{\bullet}ClO. \quad \text{(Reaction5)}$$

In this work we have extended this study to human myeloperoxidase (MPO) and bovine lactoperoxidase (LPO). The fact that MPO is involved in the regulation of immune functions [13] and that commercially

* Corresponding author. Tel.: +43 1 47654 6073; fax: +43 1 47654 6059.
E-mail address: christian.obinger@boku.ac.at (C. Obinger).

http://dx.doi.org/10.1016/j.jinorgbio.2014.02.010

available wound healing and immunomodulatory drug solutions like Oxoferin and WF10 contain chlorite as the active principle [14], prompted us to this study.

In contrast to plant-type peroxidases the heme in MPO is covalently attached to the protein via two ester-linkages and a sulfonium ion linkage [15]. These posttranslational modifications significantly modify the spectral and redox properties of this oxidoreductase, e.g. allowing MPO to oxidize chloride to hypochlorous acid that acts as antimicrobial agent in the innate immune system [16]. Additionally, the covalent heme to protein bonds were proposed to protect the heme of MPO from its highly reactive reaction products [17].

Here we demonstrate that – in contrast to horseradish peroxidase (HRP) – human MPO and bovine LPO cannot utilize chlorite to form chlorinating species [6]. Moreover, we show that both peroxidases are very susceptible to chlorite resulting in fast loss of activity accompanied by (almost) complete heme bleaching. We report the first comprehensive study of the reactions of all biological relevant redox intermediates (ferric state, Compounds I & II) of MPO and LPO with chlorite and their potential reaction products. We propose a mechanism of interaction between chlorite and the metalloproteins, discuss the observed differences with plant-type peroxidases as well as the biological relevance of our findings.

2. Material and methods

2.1. Reagents

Standard chemicals and biochemicals were obtained from Sigma-Aldrich Handels GmbH (Vienna, Austria) at the highest grade available. Hydrogen peroxide concentration was determined spectrophotometrically using an extinction coefficient at 240 nm of 39.4 M^{-1} cm^{-1} [18]. The concentration of sodium chlorite (Sigma, 80%) and hypochlorite were determined using the extinction coefficient at 260 nm of 154 M^{-1} cm^{-1} [19] and at 292 nm of 350 M^{-1} cm^{-1} [20], respectively. Highly purified dimeric leukocyte myeloperoxidase of a purity index (A_{428}/A_{280}) of at least 0.85 was purchased as lyophilized powder from Planta Natural Products (http://www.planta.at) and the concentration was determined spectrophotometrically using ε_{428} = 91 000 M^{-1} cm^{-1} per heme [21]. Lactoperoxidase from bovine milk was purchased as a lyophilized powder (Sigma, purity index A_{412}/A_{280} = 0.9). Enzyme concentration was determined by using the extinction coefficient 112,000 M^{-1} cm^{-1} at 412 nm [22]. Horseradish peroxidase type VIa was obtained from Sigma and used without further purification. An extinction coefficient at 403 nm of 102,000 M^{-1} cm^{-1} [23] was used for the determination of protein concentration. Oxovasin was obtained from NUVO Manufacturing GmbH (Wanzleben, Germany). Essentially the same drug is also marketed as Oxoferin™, a term more frequently used in a scientific context, therefore we will also refer to Oxoferin instead of Oxovasin in this study.

2.2. Preparation of chlorine dioxide

Chemically pure, chlorine free chlorine dioxide ($^{\bullet}ClO_2$) solutions were prepared by acidification of sodium chlorite (NaOClO) with sulfuric acid (H_2SO_4) according to $4\,NaOClO + 2\,H_2SO_4 \rightarrow 2\,^{\bullet}ClO_2 + HCl + HOClO_2 + 2\,Na_2SO_4 + H_2O$ [12]. In detail, 100 mL sodium chlorite (2.5% $^{w}/_{w}$) was acidified with 10 mL sulfuric acid (10% $^{v}/_{v}$). Sulfuric acid was added in 1 mL portions with 5 min intervals. Formed gaseous $^{\bullet}ClO_2$ was removed from the reaction flask by a nitrogen flow, purified by bubbling through a gas scrubbing tower containing 100 mL sodium chlorite solution (2.5% $^{w}/_{w}$) and, finally, recovered by absorbing in 100 mL chilled deionized water in an amber reagent bottle. The concentration of $^{\bullet}ClO_2$ was determined using an extinction coefficient at 359 nm of 1230 M^{-1} cm^{-1} [24]. The obtained stock solution (≈42 mM) was immediately aliquoted in Eppendorf tubes and stored in the dark at −30 °C. After thawing the stock solution was kept in the dark on ice and was stable for about 4 h. More diluted solutions were prepared immediately before use and the concentrations were determined simultaneously to the measurements.

2.3. In gel activity staining

For in-gel heme staining MPO samples (10 μg) were separated using SDS-PAGE electrophoresis under non-reducing conditions. Gels were incubated with a mixture of 6.3 mM 3,3,5,5,-tetramethylbenzidine (TMB) in methanol (3 parts) and 0.25 M sodium acetate at pH 5.0 (7 parts) for 1 h in the dark. Activity staining was started by adding hydrogen peroxide at a final concentration of 30 mM [25].

2.4. Activity assays

Monochlorodimedon (MCD) is a substrate often used to study halogenation reactions. Upon chlorination to dichlorodimedon (DCD) it loses its absorbance at 290 nm [26]. Monochlorodimedon (100 μM) and various amounts of chlorite were dissolved in 100 mM phosphate buffer, pH 5.0, and the reaction was started by addition of MPO or LPO.

For the determination of the inhibitory effect of chlorite on the chlorination activity of MPO assays contained additional hydrogen peroxide (100 μM) and chloride (100 mM). In this case the reaction was started either with MPO (100 nM) or hydrogen peroxide. The latter case resulted in a preincubation of MPO with both chloride and chlorite for 1 min.

Additionally, the inhibitory effect of chlorite on the chlorination activity was measured by continuously monitoring hydrogen peroxide concentration polarographically with a platinum electrode covered with a hydrophilic membrane and fitted to the Amperometric Biosensor Detector 3001 (Universal Sensors, Inc., U.S.A.). Again the reaction was started by adding either MPO (100 nM) or hydrogen peroxide (100 μM) after one minute. All reactions were performed at 25 °C.

As a further method to study the inhibitory effect of chlorite on MPO we used aminophenyl fluorescein (APF) which specifically detects the halogenating enzyme activity [27]. Briefly, 10 nM MPO was preincubated with 0–500 μM chlorite in phosphate buffered saline (PBS), pH 7.4, at 37 °C for 1 min. All samples also contained 10 μM APF. The enzymatic activity was started by adding 25 μM H_2O_2 via an injector device. The HOCl-derived oxidation of APF was followed for 30 min at 37 °C by measuring the fluorescence intensity at 522 nm (excitation at 488 nm). All measurements were performed in a fluorescence microplate reader Tecan Infinite 200 PRO, Switzerland.

2.5. Circular dichroism and electron paramagnetic resonance spectroscopy

Circular dichroism spectra (CD) were recorded using a Chirascan CD spectrophotometer (Applied Photophysics, UK). In the far-UV region an enzyme concentration of 2 μM and a cuvette with a path length of 1 mm was used. For measurements in the Soret region (300 nm–500 nm) the enzyme concentration was 5 μM and the path length of the cuvette was 1 cm.

Samples for electron paramagnetic resonance (EPR) measurements were prepared using 100 μM MPO in 100 mM phosphate buffer, pH 5. After addition of chlorite in 5- and 10-fold excess, respectively, 5% glycerol was added as cryoprotectant and 100 μL of the reaction solution were immediately transferred into a quartz EPR tube (4 mm OD) and frozen in liquid nitrogen. Before measurement, the tube was degassed with Ar while the sample was kept frozen on dry ice.

EPR measurements were carried out at 10 K on an EMX continuous wave (cw) spectrometer (Bruker, Germany), operating at X-band (9 GHz) frequencies, equipped with a high sensitivity resonator and a helium cryostat from Oxford Instruments (ESR900). EPR spectra were recorded under non-saturating conditions using 2 mW microwave power, 100 kHz modulation frequency, 1 mT modulation amplitude, 20 ms conversion time and 20 ms time constant and 4096 data points. Simulations of high-spin Fe(III) spectra were carried out using the

software EasySpin [28] and consist of a weighted sum of simulations of the individual high-spin intermediates.

2.6. Transient state kinetics

Transient-state measurements were made using the SX.18 MV stopped-flow spectrophotometer and PiStar-180 circular dichroism spectrometer (Applied Photophysics, UK) equipped with a 1 cm observation cell. Calculation of pseudo first-order rate constants (k_{obs}) from experimental time traces was performed with a SpectraKinetic work station (Version 4.38) interfaced to the instruments. Second-order rate constants were calculated from the slope of the linear plot of the pseudo first-order rate constants versus substrate concentration. To follow spectral transitions, a Model PD.1 photodiode array accessory (Applied Photophysics, UK) connected to the stopped-flow machine together with XScan diode array scanning software (Version 1.07) was utilized.

2.7. Differential scanning calorimetry

Differential scanning calorimetric (DSC) measurements were performed using a VP-capillary DSC microcalorimeter from Microcal (cell volume: 137 μL), controlled by the VP-viewer program and equipped with an autosampler for 96 well plates. Samples were analyzed using a programmed heating scan rate of 60 °C h^{-1} over a temperature range of 20 °C to 110 °C and a cell pressure of approximately 60 psi (4.136 bar). Collected DSC data were corrected for buffer baseline and normalized for protein concentration. The reaction conditions were: 5 μM MPO in 100 mM phosphate buffer pH 5.0 in the absence or presence of 25 μM chlorite and different incubation times. Reactions were stopped by addition of 4 mM cysteine. Guanidinium hydrochloride (GdnHCl; 5 mM) was added before measurements were started to avoid non-specific protein aggregation at increasing temperatures.

Microcal origin software was used for data analysis. Heat capacity (C_p) was expressed in kcal mol^{-1} K^{-1} (1 cal = 4.184 J). Data points were fitted to non-two-state equilibrium-unfolding models by the Lavenberg/Marquardt (LM) non-linear least square method.

3. Results

The plant-type model peroxidase HRP is able to use chlorite instead of hydrogen peroxide as two-electron oxidant of the ferric state, thereby forming Compound I and hypochlorous acid [12], which is known to chlorinate various target molecules like MCD. In contrast, as already observed by George [6], no chlorinating species could be detected in the reaction between MPO with chlorite. Upon re-evaluation of this reaction we could confirm that the system MPO/chlorite is unable to chlorinate MCD (not shown). This significant discrepancy between plant-type peroxidases and their mammalian counterparts prompted us to perform a more comprehensive study on (i) the interaction of chlorite with all relevant redox intermediates of MPO and LPO as well as on (ii) the impact of chlorite on their structural integrity.

3.1. Reaction of ferric MPO and LPO with chlorite

Upon reaction of chlorite with ferric MPO the heme absorbance in the Soret region rapidly decreased. Fig. 1A and B depict the spectral changes upon addition of 200 μM chlorite to 2 μM ferric MPO at pH 5.0. The reaction was biphasic (inset to Fig. 1A), with the first rapid phase (Fig. 1A) leading directly (isosbestic points at 445 nm, 490 nm, 595 nm and 660 nm) to an intermediate state within 60 ms. This state (gray spectrum in Fig. 1A) exhibited a decreased absorbance at the Soret maximum as well as a shoulder around 455 nm (isosbestic point at 445 nm), which was more pronounced at higher chlorite concentrations. Concomitant spectral changes at higher wavelengths in the visible region included absorbance decrease at 570 nm and increase at 625 nm

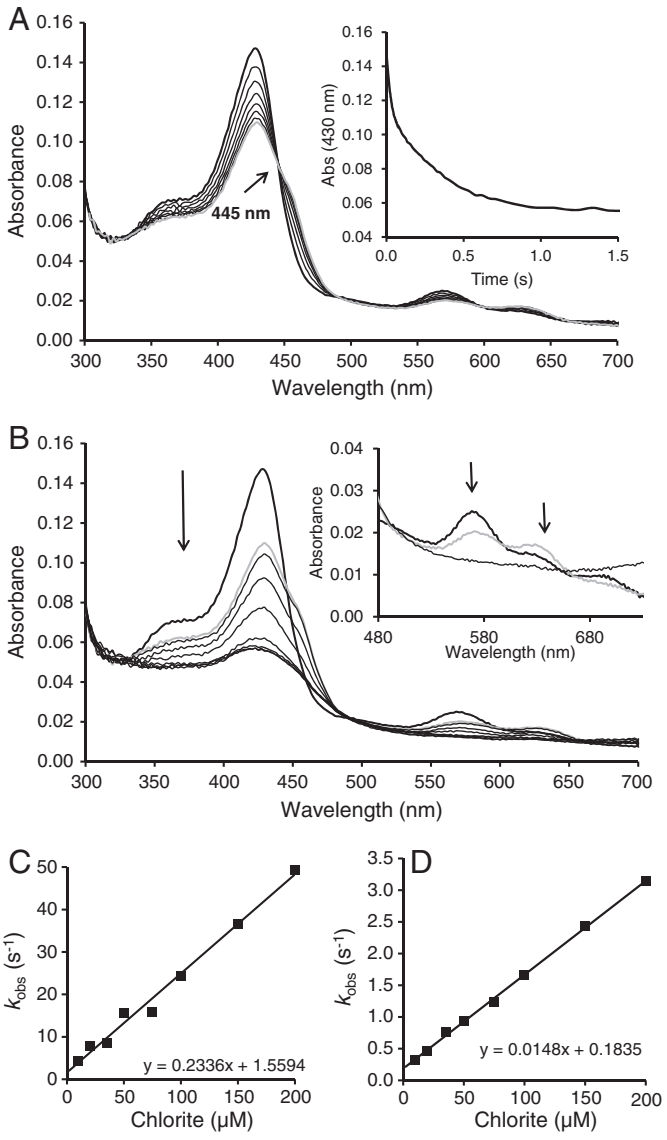

Fig. 1. Reaction of ferric MPO with chlorite. Assay: 2 μM MPO with 200 μM chlorite in 100 mM phosphate buffer, pH 5.0. (A) Spectral changes observed within the first 60 ms. Black spectrum, ferric MPO; and gray spectrum, intermediate observed after 60 ms. The inset shows the corresponding biphasic time trace at the Soret maximum for the first 1.5 s. (B) Continuation of reaction in (A). Gray spectrum corresponds to gray spectrum in (A). Subsequent spectra (black) were taken at 80 ms, 170 ms, 350 ms, 710 ms, 1.5 s and 10 s, respectively. For orientation the spectral features of ferric MPO (bold black) are included. (C) Plot of the pseudo-first-order rate constants against chlorite concentration for the fast phase of the reactions. (D) Plot of the pseudo first-order rate constants against chlorite concentration for the second slower phase.

(isosbestic points at 492 and 593 nm). The second and slower phase (Fig. 1B) was characterized by a continuous loss of absorbance in the whole spectral region between 300 and 650 nm.

Upon fitting of this biphasic reaction by using a double exponential equation apparent bimolecular rate constants were calculated. Both phases were dependent on the concentration of chlorite. Fig. 1C and D show the resulting plots of the respective pseudo-first order rate constants against substrate concentration yielding second order rate constants of 2.3×10^5 M^{-1} s^{-1} (fast reaction) and 1.5×10^4 M^{-1} s^{-1} (slow reaction) at pH 5.0. Both reactions strongly depended on the pH. The second-order rate constants at pH 4.0 were roughly one order of magnitude higher compared to pH 5.0 (1.5×10^6 M^{-1} s^{-1} and 8.4×10^4 M^{-1} s^{-1}), whereas at pH 7.0 rate constants of 4.6×10^4 M^{-1} s^{-1} and 3.1×10^3 M^{-1} s^{-1}, respectively, were obtained.

Fig. 2A shows an overlay of the spectrum of 1 μM ferric MPO at pH 5 (black line) and the final absorbance spectrum after reaction with 50 μM chlorite (gray line). Heme bleaching at the Soret band was accompanied by a substantial increase in absorbance in the region between 650 and 850 nm and the appearance of maxima at 700 nm and 754 nm (inset to Fig. 2A). To our knowledge these spectral features have never been reported so far for MPO and most probably indicate heme destruction and the formation of an inactive form similar to the P670 species in HRP [29]. Fig. 2B shows a typical time trace of the reaction of 2 μM MPO with 1 mM chlorite at pH 5.0 followed at 720 nm. The reaction was monophasic and could be fitted using a single exponential equation and the plot of the pseudo-first order rate constants against chlorite concentration yielded a straight line (Fig. 2C). From the slope an apparent second order rate constant of $4.8 \times 10^3\ M^{-1}\ s^{-1}$ could be calculated. Again this reaction was pH dependent with $9.1 \times 10^4\ M^{-1}\ s^{-1}$ and $1.5 \times 10^3\ M^{-1}\ s^{-1}$ at pH 4.0 and 7.0, respectively. These rate constants were similar to those obtained for the slow phase of the biphasic reaction depicted in Fig. 1 and might reflect modification and destruction of the prosthetic group.

In order to probe the nature of the initial binding complex (the transition with clear isosbestic points, Fig. 1A) between ferric MPO and chlorite, EPR spectroscopy was performed. Fig. 3A shows the spectrum of 100 μM ferric MPO in 100 mM phosphate buffer, pH 5.0, reflecting a predominantly rhombically distorted high-spin form with some small contributions of less rhombicity. Similar spectra were recorded previously [30]. Already upon preincubation of MPO with a very low excess of chlorite (5-times stoichiometric excess) the rhombicity significantly changed, indicating a rearrangement around the heme center towards axial symmetry (Fig. 3B). Since formation of a low-spin species was not detected, chlorite seemed to act as high-spin ligand. This became

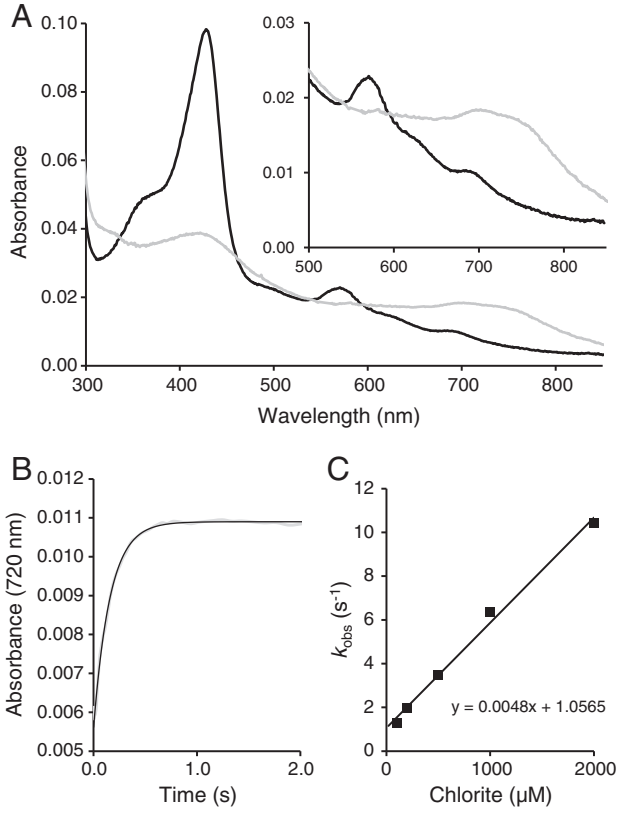

Fig. 2. Kinetics of heme degradation. (A) Comparison of spectral features of 1 μM ferric MPO (black) with the spectral features obtained upon reaction of 1 μM MPO with 50 μM chlorite (gray) at pH 5.0. (B) Time trace at 720 nm and single exponential fit for the reaction of 2 μM MPO with 1 mM chlorite at pH 5.0. (C) Plot of the obtained pseudo-first-order rate constants against chlorite concentration.

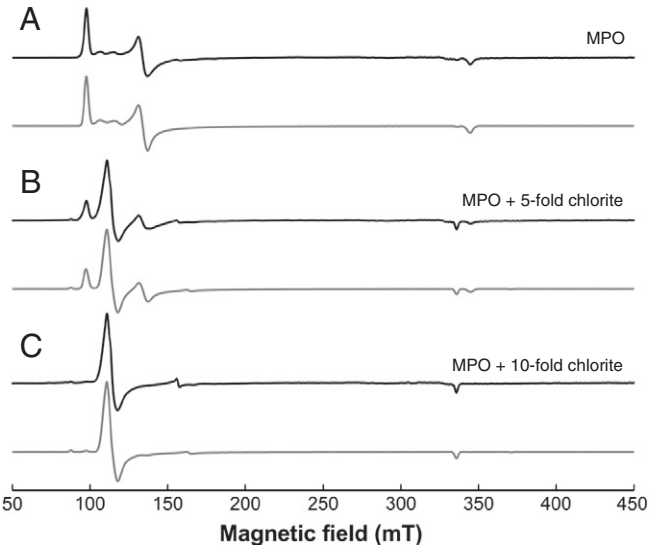

Fig. 3. EPR analysis of the interaction of MPO with chlorite. Experimental cw EPR spectra (black) and simulation (gray) of (A) 100 μM ferric MPO in 100 mM phosphate buffer, pH 5.0, (B) 100 μM MPO after addition of 5-fold chlorite and (C) 100 μM MPO after addition of 10-fold chlorite. The spectra were recorded at 10 K and the samples contained 5% glycerol.

further evident by preincubation of MPO with a higher (10-fold) excess of chlorite (Fig. 3C). Here, the rhombically distorted high-spin forms disappeared almost completely leading to a predominantly axial signal. Table 1 shows the simulation parameters of the individual high-spin forms as well as their rhombicity and intensity fraction based on the simulation. Again, a low-spin species could not be detected. Moreover, with increasing chlorite concentrations the intensity at $g = 4.3$ increased slightly (compare Fig. 3A and C) reflecting the release of non-heme Fe(III).

Next we tested another member of the vertebrate peroxidase subfamily [31], namely bovine LPO, in its interaction with chlorite. Lactoperoxidase was also unable to utilize chlorite in MCD chlorination (data not shown) and was even faster inactivated by chlorite than MPO. The reaction between LPO and chlorite was again biphasic (Supplemental Fig. 1). Upon mixing of 1 μM ferric LPO with 100 μM chlorite at pH 5.0, a rapid spectral transition occurred within the first 20 ms (isosbestic point at 425 nm), resulting in a decrease in absorbance of the Soret band which was accompanied by a small red shift of the Soret maximum (Supplemental Fig. 1A). This fast transition was followed by a slower reaction leading to a further loss of absorbance in the Soret region within 400 ms (Supplemental Fig. 1B). Interestingly, and in contrast to MPO, this second transition showed an isosbestic point at 448 nm before heme bleaching occurred. The loss of absorbance at the Soret maximum and the charge transfer bands during heme

Table 1
EPR simulation parameters from individual high spin forms of MPO with chlorite (HS — high-spin, R — rhombicity, I — relative intensity, E/D — rhombic to axial contribution).

	HS compounds*	g_x^{eff}	g_y^{eff}	g_z^{eff}	E/D	R (%)	I (%)
Ferric MPO	HS1	5.000	6.660	1.945	0.040	12	94
	HS2	5.700	6.300	1.995	0.013	4	6
Ferric MPO +	HS1	4.100	7.650	1.945	0.079	22	4
5-fold chlorite	HS2	5.000	6.880	1.945	0.040	12	50
	HS3	5.750	6.200	1.998	0.006	3	45
	HS4	5.890	6.050	1.998	0.003	1	2
Ferric MPO +	HS1	4.100	7.650	1.945	0.079	22	8
10-fold chlorite	HS2	5.000	6.880	1.945	0.040	12	5
	HS3	5.750	6.200	1.998	0.006	3	84
	HS4	5.890	6.050	1.998	0.003	1	4

* Minimum number of high-spin compounds used for simulation.

bleaching was accompanied by a broad increase of absorbance in the range of 600–850 nm with two clear peaks with maxima at 650 nm and 730 nm (Supplemental Fig. 1E).

Analysis of the time traces at 412 nm and double exponential fitting yielded bimolecular rate constants of 2×10^6 M^{-1} s^{-1} (fast transition) and 7.7×10^4 M^{-1} s^{-1} (slower transition) at pH 5.0 (Supplemental Fig. 1C & D). Both rates were significantly faster compared to MPO. Again this reaction was pH dependent. At pH 7.0 both rate constants were about one order of magnitude lower (1.1×10^5 M^{-1} s^{-1} and 4×10^3 M^{-1} s^{-1}, respectively).

3.2. Influence of cyanide and chloride on heme bleaching mediated by chlorite

Cyanide is known to bind directly to the Fe(III) center of heme peroxidases [32]. Ferric MPO (2 μM) was incubated with 10 mM cyanide resulting in the formation of a low-spin complex, characterized by a red shift of the Soret band of MPO to 455 nm and formation of a prominent peak at 635 nm (black spectrum in Fig. 4A). Upon addition of chlorite to the cyanide complex of MPO no spectral changes were observed even at high chlorite concentrations and prolonged measurements (Fig. 4A, gray trace, final concentration 500 μM chlorite). No heme bleaching was observed. This suggests that the presence of cyanide hampers the attack of the heme iron and/or the prosthetic group by chlorite.

Since chloride acts both as high-spin ligand and substrate of MPO [33], we have also probed the effect of chlorite on the MPO-Cl^- complex. At pH 5.0 the spectrum of the latter shows a Soret maximum at 435 nm and a Q-band at 574 nm. Myeloperoxidase was incubated with 100 mM chloride at pH 5.0 before chlorite was added. Fig. 4B shows the spectral changes of the reaction between 2 μM MPO-chloride complex and 200 μM chlorite. In contrast to cyanide the presence of chloride did not protect MPO from heme bleaching. However, compared to native MPO clear differences were observed. The reaction was slower and monophasic (Fig. 4C). The absence of a shoulder at 455 nm as well as of an absorbance increase at 625 nm (compared to Fig. 1A) suggests that the presence of chloride had an influence on the velocity of the formation of the (high-spin) MPO-chlorite complex but not on the final heme degradation. The presence of chloride did slow down binding of chlorite and the reaction lost its biphasic behavior. Heme bleaching was still evident from the observed increase of absorbance in the long wavelength range (600–850 nm). This hypothesis is underlined by the fact that the rate constant of absorbance loss at 430 nm of 2.5×10^3 M^{-1} s^{-1} (Fig. 4D) corresponded well to the rate of absorbance increase at 720 nm, i.e. 4.8×10^3 M^{-1} s^{-1} (see also Fig. 2C).

For HRP we could demonstrate, that chlorine dioxide (besides chlorite) mediates Compound I formation [12]. By contrast, neither ferric MPO nor ferric LPO reacted with chlorine dioxide at pH 5.0 and 7.0. No heme bleaching was observed and the spectral features of both enzymes remained unchanged (data not shown).

3.3. Reactions of Compound I and Compound II of MPO and LPO with chlorite

In the next step the reaction of preformed MPO Compound I with chlorite was investigated by multi-mixing stopped-flow spectroscopy. In contrast to ferric MPO, Compound I reacted very fast with chlorite forming Compound II, which was further converted back to ferric MPO (Fig. 5). Fig. 5A depicts the spectral changes of the reaction between 2 μM MPO Compound I and 20 μM chlorite at pH 5.0. Compound II was formed rapidly (Soret maximum at 455 nm and a dominant peak at 625 nm). The first recorded spectrum 1.3 ms after mixing (black bold spectrum) already showed a significant amount of Compound II and the reaction was completed within 15 ms (gray spectrum). From the monophasic time traces at 455 nm a bimolecular rate constant of 1.2×10^7 M^{-1} s^{-1} was calculated (Fig. 5B and C). The rate decreased with increasing pH, i.e. 1.7×10^6 M^{-1} s^{-1} at pH 7.0.

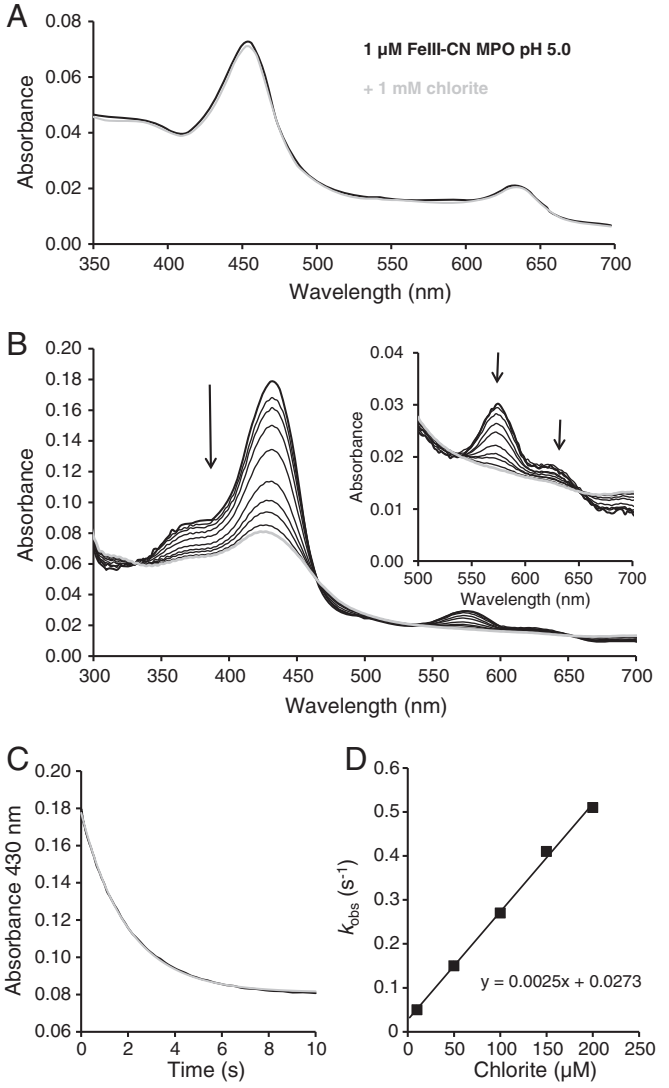

Fig. 4. Impact of ligands on the interaction of MPO and chlorite. (A) 2 μM ferric MPO was preincubated with 10 mM cyanide prior to mixing with 500 μM chlorite (final enzyme concentration 1 μM) at pH 5.0. First spectrum collected after 1.3 ms (black) corresponds to the low-spin complex of MPO. Even 10 s after mixing with chlorite no changes in the spectral features were detected (gray spectrum). (B) 4 μM ferric MPO at pH 5.0 was pre-incubated with 100 mM chloride prior to mixing with 200 μM chlorite (final enzyme concentration 2 μM) at pH 5.0. First spectrum was taken after 5 ms (bold), subsequent spectra at 163 ms, 317 ms, 592 ms, 1.1 s, 2.1 s, 3.1 s, 4.1 s, 6.2 s and 10 s (gray spectrum). The inset shows an enlargement of the visible region from 500 to 700 nm for the same reaction. (C) Time trace at 430 nm (black) including single-exponential fit (gray) for the reaction in (B). (D) Plot of pseudo-first-order rate constants versus chlorite concentration.

Compound II was not stable but reacted back to ferric MPO dependent on the chlorite concentration (Fig. 5D is a continuation of Fig. 5A) within 700 ms (isosbestic points at 441 nm, 490 nm, 585 nm and 670 nm). Exact determination of the bimolecular rate constant was not possible due to the fact that excess of chlorite immediately reacted with any formed ferric enzyme resulting in heme bleaching. Estimated values for Compound II reduction were 1.4×10^5 M^{-1} s^{-1} at pH 5.0 and 3×10^4 M^{-1} s^{-1} at pH 7.0, respectively.

Similarly, Compounds I and II of LPO were probed in their reactivity with chlorite. Clear monophasic transitions (without heme bleaching during these distinct redox transformations) were observed. Supplemental Fig. 2A shows the reaction between 2 μM Compound I and 5 μM chlorite to Compound II (Soret maximum at 428 nm and two peaks at 536 nm and 566 nm) at pH 7.0. The bimolecular rate constant was calculated to be 5.8×10^6 M^{-1} s^{-1} at pH 7.0. The spectral features obtained in these reactions did not resemble a pure Compound II but did

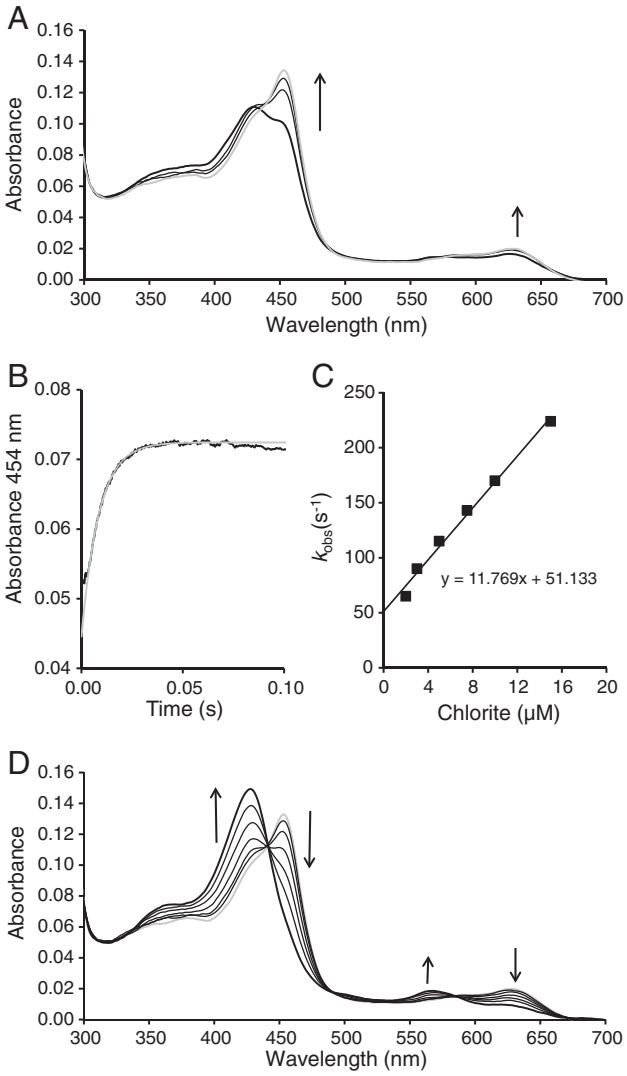

Fig. 5. Reactions of MPO Compounds I and II with chlorite. (A) 2 μM MPO Compound I was pre-formed with a 10-fold excess of hydrogen peroxide (pH 5.0) and – after a delay time of 20 ms – chlorite at a concentration of 20 μM was added. First spectrum (bold) was taken at 1.3 ms, subsequent spectra at 4 ms, 6 ms and 15 ms (gray spectrum). (B) Plot of pseudo-first-order rate constants for Compound I reduction versus chlorite concentrations. (C) Time trace at 454 nm and single-exponential fit for the reaction of 1 μM MPO Compound I with 5 μM chlorite. (D) Continuation of reaction in (A) showing the reduction of Compound II by chlorite. Gray spectrum corresponds to Compound II (15 ms, as in A) and subsequent spectra were taken at 100 ms, 200 ms, 300 ms, 500 ms and 700 ms (black bold spectrum).

already contain a shoulder caused by the formation of ferric LPO due to the reaction of Compound II with chlorite.

Finally, Compound II of LPO (pre-formed by mixing of 8 μM LPO with 12 μM hydrogen peroxide and 40 μM tryptophan in the aging loop and setting a delay time of 2 s) [34] was directly converted to ferric LPO by chlorite with a rate constant of 4.4×10^4 M^{-1} s^{-1} at pH 7.0 (Supplemental Fig. 2B). However, as already observed with MPO, ferric LPO was not formed completely as it reacted immediately with excess chlorite leading to heme destruction.

3.4. Impact of chlorite on the overall halogenation activity of MPO

As mentioned at the beginning, the system of MPO/chlorite (in contrast to HRP/chlorite) was not able to promote monochlorodimedon chlorination, suggesting that hypochlorous acid was not formed or at least could not leave the heme cavity or immediately reacted with the heme or neighboring amino acids of the protein. Hypochlorous acid is well known to mediate Compound I formation of MPO [35] as well as to promote degradation of the heme group [36]. Thus, in order to exclude a role of HOCl in the observed heme bleaching reaction mediated by chlorite, we have probed the impact of 10 mM methionine on the inactivation process. Methionine is small enough to enter the substrate channel and it reacts very fast with HOCl [37]. However, with both MPO and LPO, the presence of methionine did not prevent heme bleaching (data not shown). Similarly addition of taurine, another very efficient trap for hypochlorous acid, showed no effect on the spectral transitions.

Next, the inhibitory effect of chlorite on the chlorination activity of MPO was determined. At pH 5.0 the effect was investigated both spectrophotometrically (monitoring the chlorination of MCD to DCD at 290 nm) and polarographically (monitoring consumption of hydrogen peroxide).

In order to exclude a possible impact of MCD as potential one-electron substrate for MPO Compounds I and II on the reaction, the effect of chlorite was in addition determined fluorimetrically (monitoring the chlorination of APF at pH 7.4). The reactions were started by addition of either MPO or hydrogen peroxide, in the latter case MPO was preincubated with chlorite for 1 min.

Independent of the method used the inhibitory effect was stronger when MPO was preincubated with chlorite and the reaction was started with hydrogen peroxide. A concentration of ~15 μM of chlorite resulted in a loss of 50% activity (Fig. 6A & B) when MPO was preincubated with chlorite. When the reaction was started with native MPO much higher concentrations of chlorite (40–50 μM) were necessary to obtain 50% inhibition (Fig. 6C & D). These observations underline that only MPO in its ferric state is susceptible to degradation by chlorite. Similar to high-spin (chloride) or low-spin (cyanide) ligands the substrate hydrogen peroxide binds to the sixth heme position and protects or at least delays inactivation by chlorite.

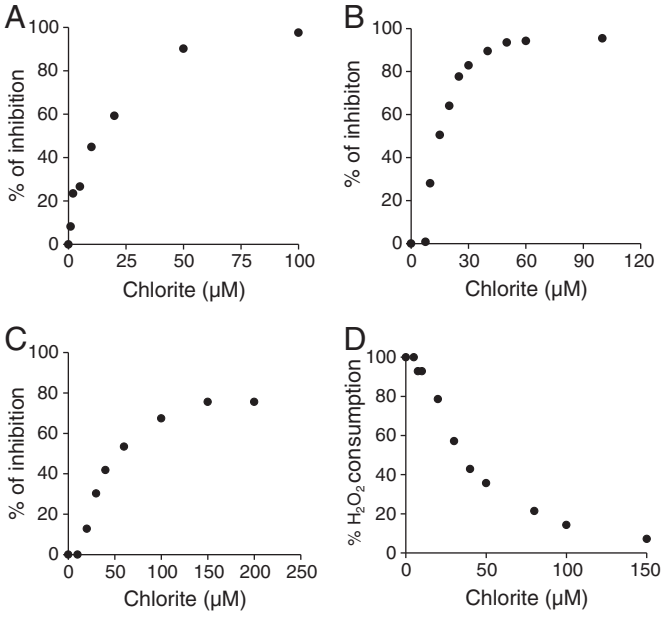

Fig. 6. Inhibition of chlorination activity of MPO by chlorite. Activity was monitored either by APF chlorination fluorimetrically (A), monochlorodimedon (MCD) chlorination spectrophotometrically (B, C) or by monitoring hydrogen peroxide consumption polarographically (D). In (A) and (B) MPO was incubated with various concentrations of chlorite for one minute and the reaction was started by adding hydrogen peroxide. In (C) and (D) the reaction was started by adding native MPO to the reaction mixture. For detailed reaction conditions see Material and methods.

3.5. Effect of chlorite on the structural integrity of MPO

Chlorite-mediated heme destruction could readily be detected by in-gel activity heme staining after samples were run on a non-reducing SDS-PAGE. Human MPO (10 μg) was mixed with increasing concentrations of chlorite (Fig. 7A; lane 2–5: 0, 50, 200 and 500 μM chlorite, respectively) at pH 5.0 and loaded on the gel followed by activity staining. Addition of chlorite decreased the color development in a concentration dependent manner (Fig. 7A), proofing the loss of active heme.

On a separate gel the same amount of MPO and chlorite were run on a non-reducing SDS-PAGE and stained by Coomassie (Fig. 7B). Myeloperoxidase predominantly ran as a dimer (lane 2) but upon mixing with chlorite a second protein band at ~14 kDa appeared, which corresponds to the light chain of MPO. The more chlorite was added to MPO, the more pronounced was this band (Fig. 7B; lanes 3–5). Additionally, diffuse protein bands with high molar masses were formed (lane 5), indicating either protein aggregation or crosslinked multimeric states of MPO.

For comparison, Fig. 7C depicts the SDS-PAGE of the same sample preparations under reducing conditions [50 mM dithiothreitol (DTT) was added to the samples]. Here, two prominent bands of MPO appeared, corresponding to its heavy (60 kDa) and light chains (14 kDa). No differences between untreated and chlorite-treated samples were detected indicating that the chlorite dependent decrease in heme activity staining was not due to loss of protein.

To further evaluate the effect of chlorite on the secondary structure composition of MPO CD spectroscopy in the far-UV region was performed. Fig. 8A shows identical CD spectra of 2 μM native MPO (pH 5.0) and 2 μM MPO after treatment with 1 mM chlorite at 25 °C. The CD spectra consisted of two minima at 208 and 222 nm, which are typical for a mainly α-helical structure. Even upon longer incubations of MPO with this huge excess of chlorite (500-times) only a very slight loss of ellipticity was observed. Obviously, chlorite did not have any impact on the overall secondary structure composition of MPO at room temperature.

Next we investigated the effect of chlorite on the heme ellipticity in the Soret region at room temperature. Ferric MPO showed a negative ellipticity with a minimum around 412 nm in the Soret region (Fig. 8B, black line). Upon binding of moderate (20-times) excess of chlorite the signal changed dramatically resulting in alteration of the sign of ellipticity (Fig. 8B, gray line). This indicates that (i) the heme was still attached to MPO under these conditions (free heme does not show an CD signal) and (ii) that upon chlorite binding the interaction of the prosthetic group and its (asymmetric) protein environment was significantly modified [38]. By contrast, simultaneous measurements of the Soret maximum at 430 nm by UV–vis spectroscopy showed an almost complete loss of absorbance in this region (Fig. 8C).

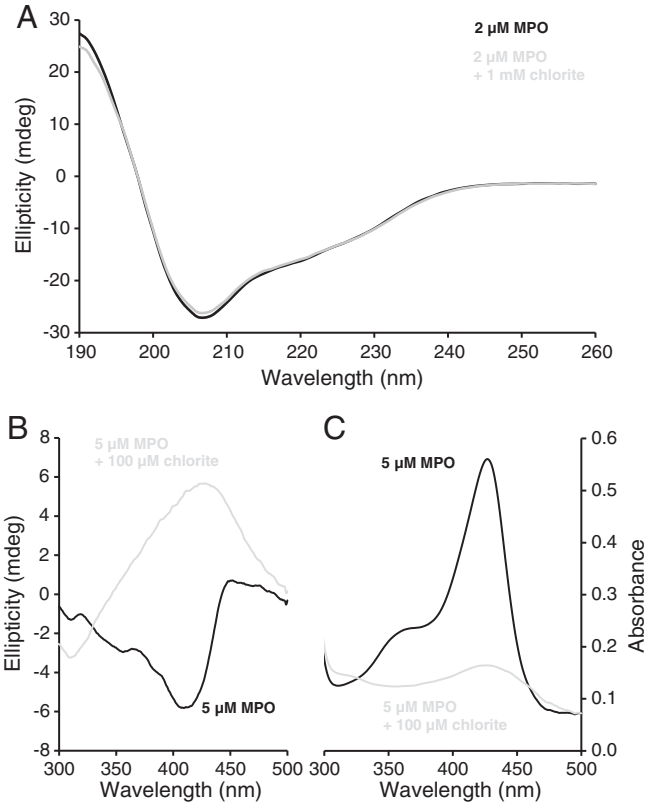

Fig. 8. Circular dichroism analysis. (A) Far-UV CD spectra of native MPO (black) MPO incubated with chlorite (gray) at pH 5.0. Protein concentration: 2 μM; and chlorite concentration: 1 mM. Path length: 1 mm. (B) CD spectra in the Soret region of native MPO and chlorite treated MPO at pH 5.0. Protein concentration: 5 μM; and chlorite concentration: 100 μM. Path length: 1 cm (C) Corresponding absorbance spectra of native MPO and chlorite treated MPO. Conditions as in (B).

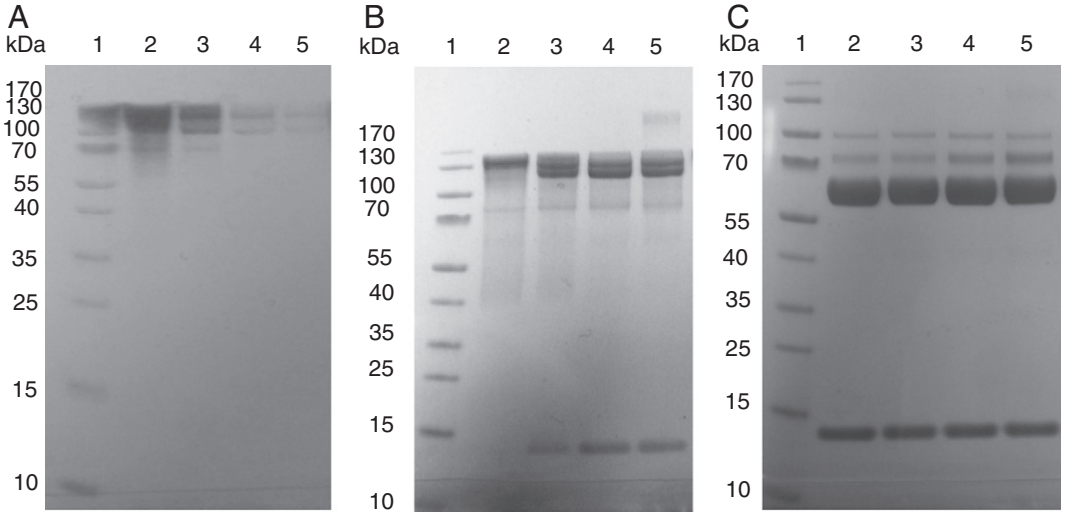

Fig. 7. SDS-PAGE analysis of MPO incubated with chlorite. (A) Non-reducing SDS-PAGE. Bands were visualized by in-gel heme staining. (B) Non-reducing SDS-PAGE. Protein bands were visualized by Commassie staining. (C) Reducing SDS-PAGE. Protein bands were visualized by Commassie staining. Lane 1, marker; lane 2, 10 μg MPO; lane 3, 10 μg MPO + 50 μM chlorite; lane 4, 10 μg MPO + 200 μM chlorite; and lane 5, 10 μg MPO + 500 μM chlorite.

Finally, calorimetric studies of the effect of chlorite on the thermal unfolding of MPO were performed. Fig. 9 shows the DSC profile of MPO in 100 mM phosphate buffer, pH 5.0. One slightly asymmetric endotherm was obtained with a maximum at T_m of 87 °C. Deconvolution of data suggests a non-two-state unfolding and two transitions at 84.5 and 87.5 °C. Upon incubation with a 5-time stoichiometric excess of chlorite for 1 min (stopping the reaction by 4 mM cysteine) a completely different unfolding pattern was obtained that clearly reflected loss of structural integrity and a diminished thermal stability. Satisfactory fitting was only possible by supposing of at least three intermediate states with calculated T_m values at 87.5, 84.5 and 73.0 °C, respectively. At longer incubation times or higher excess of chlorite, the T_m values shifted to lower temperatures and the endotherms became broad and flat (data not shown).

3.6. Comparison of chlorite with chlorite-based drugs in interaction with MPO

The drug substance OXO-K993 (NUVO Research Inc., Mississauga, Canada), also referred as tetrachlorodecaoxygen anionic complex [i.e. $(Cl_4O_{10})_n$ with molar mass of 301.8 for n = 1] contains 4.25% chlorite, 1.9% chloride, 1.5% chlorate, 0.7% sulfate and sodium ions as cationic species in an aqueous solution [14]. A sterile, pyrogen-free, aqueous 10% (w/v) solution of OXO-K993 is applied under the name WF10 for intravenous infusion in patients with chronic-inflammatory diseases [39–41]. Another 55-fold diluted formulation derived from OXO-K993 is Oxoferin™ that is topically applied as a wound-healing agent [42,43].

Here we applied Oxoferin to test the effects of this drug solution upon interaction with MPO. The chlorite content in Oxoferin is reported to be 12.3 mM [44]. To test if the additives lead to any differences in reactivity the direct reaction of human ferric MPO with this drug was investigated. The reaction of MPO with Oxoferin showed similar kinetics and finally resulted in heme bleaching (Supplemental Fig. 3). The reaction was biphasic with calculated rate constants of $3.9 \times 10^5\ M^{-1}\ s^{-1}$ and $2.3 \times 10^4\ M^{-1}\ s^{-1}$ (pH 5.0), respectively. Thus, with respect to reactivity towards MPO in terms of heme bleaching and kinetics, Oxoferin is indistinguishable from a pure chlorite solution.

4. Discussion

In the present study, we have demonstrated remarkable differences in the reaction of the mammalian peroxidases MPO and LPO with chlorite in comparison to the plant-type model peroxidase HRP. In the latter, chlorite acts as both a two-electron oxidant for the ferric enzyme forming Compound I as well as a one-electron donor for Compound I and Compound II. Two reaction products are formed, hypochlorous acid and chlorine dioxide, and both can mediate chlorination reactions. By contrast, the system MPO/chlorite is unable to perform chlorination reactions.

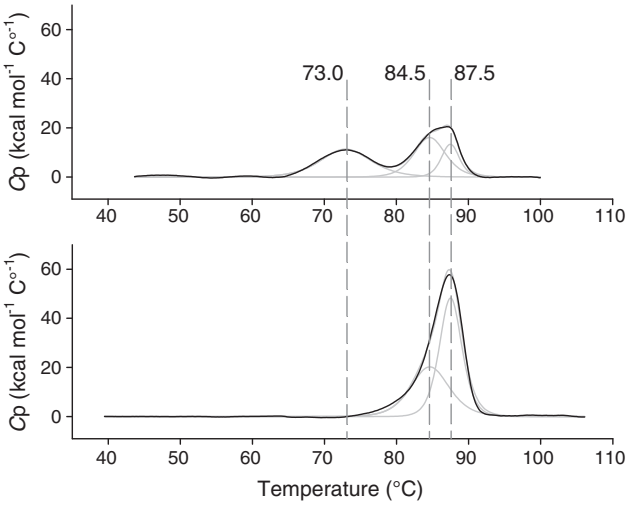

Fig. 9. Effect of chlorite on the thermostability of myeloperoxidase. Normalized DSC scans of 5 μM MPO in the absence (lower panel) or presence of 25 μM chlorite in 100 mM phosphate buffer, pH 5.0. Experimental data (black lines) and fitting to non-two-state models (gray lines) are shown.

The main difference between the mammalian peroxidases and HRP concerns the interaction of chlorite with the ferric resting state. Chlorite is well known to oxidize ferric HRP to Compound I by abstracting two electrons [12]. The standard reduction potential for the couple Compound I/ferric HRP can be calculated from data given in ref. [45] to be 0.92 V at pH 7. This value is lower than the potential for the couple ClO_2^-/HOCl, H_2O being 1.08 V at pH 7 [46], indicating the thermodynamic feasibility of HRP oxidation by chlorite. Under slightly acidic conditions, this oxidation becomes more favorable because of the divergent pH dependencies of both redox couples. The potential of the couple Compound I/ferric HRP increases by 0.59 V per decreasing pH unit, while a corresponding increase of 0.88 V is found for the couple ClO_2^-/HOCl, H_2O.

However, chlorite was unable to oxidize ferric LPO or MPO to Compound I. Instead of this, both peroxidases were inactivated by chlorite due to heme degradation. The standard reduction potentials of the redox couple Compound I/ferric enzyme are higher than for HRP at pH 7 with 1.16 V for MPO [47] and 1.09 V for LPO [34]. Considering the abovementioned pH dependencies of redox couples, an oxidation of at least ferric LPO to Compound I by chlorite can be expected at lower pH values. However, our results clearly revealed that even at pH 5 neither LPO nor MPO were oxidized by chlorite. Thus in addition, differences in the heme structure and the surrounding protein are apparently responsible for divergent chlorite effects with ferric MPO and LPO in contrast to ferric HRP. The most striking structural difference in the active site between HRP and the mammalian peroxidases is that in the latter two the heme is covalently attached to the protein (Fig. 10). The 1- and 5-methyl groups of heme pyrrole rings A and C are modified in both LPO and MPO allowing them to form ester linkages with the carboxyl group of a conserved aspartate and glutamate. In addition, in MPO a sulfonium linkage between the ß-carbon of the vinyl ring of pyrrole ring A and the sulfur atom of methionine 243 is formed [15]. Besides these heme modifications also the residues on the distal side of the heme differ between HRP and MPO/LPO. In plant-type peroxidases the triad histidine, arginine and phenylalanine is conserved, whereas the most prominent distal residues in mammalian peroxidases are histidine, arginine and glutamine, respectively (Fig. 10).

Chlorite rapidly binds at the active site forming a high-spin complex (MPO: $4.6 \times 10^4\ M^{-1}\ s^{-1}$ and LPO: $1.1 \times 10^5\ M^{-1}\ s^{-1}$ at pH 7.0) as demonstrated by (i) UV–vis stopped-flow spectroscopy, (ii) EPR-spectroscopy, and (iii) the impact of cyanide and chloride on this reaction. After binding of chlorite heme degradation occurred (MPO: $1.5 \times 10^3\ M^{-1}\ s^{-1}$ and LPO: $4.0 \times 10^3\ M^{-1}\ s^{-1}$ at pH 7.0) leading to loss of Soret absorbance and partial iron release. New absorbance bands in the region 600–800 nm indicate the formation of heme degradation product(s). The pH-dependence of both reactions (chlorite binding and heme bleaching) suggests that apparently HOClO, the protonated form of chlorite, is the reactive species. The pK_a value of HOClO is 1.72 [48].

In contrast to the ferric state, Compounds I and II of MPO and LPO are able to oxidize chlorite in a one-electron step as was previously observed for HRP [12]. However, rate constants for these transitions are much higher for MPO and LPO than for HRP in the pH range from 4 to 7. For all three peroxidases, these rate constants increase with decreasing pH. In addition to structural aspects determining the binding of chlorite near the heme, thermodynamic considerations play also a role in this divergent behavior. The standard reduction potential of the couple ClO_2/ClO_2^- has a value of 0.934 V and is independent of pH at pH values higher than 2 [49]. The reduction potential for the couple

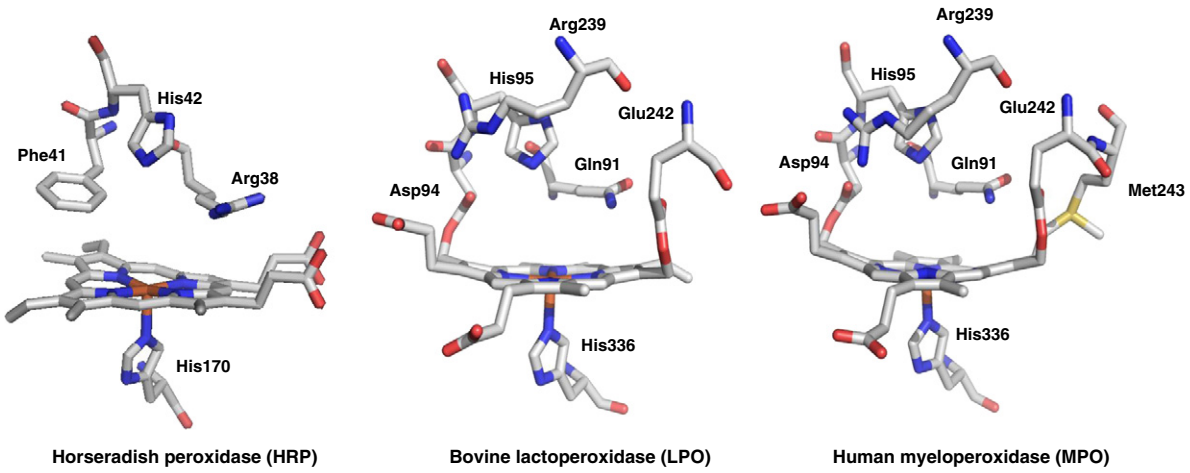

Fig. 10. Active site structure of HRP, bovine LPO and human MPO. The figures were constructed using the coordinates deposited in the Protein Data Bank. Accession codes: 1ATJ (HRP), 1CXP (MPO) and 2GJM (LPO).

Compound I/Compound II for HRP can be calculated to be 0.91 V at pH 7 [12]. The corresponding $E^{\circ\prime}$ values for MPO and LPO at pH 7 are significantly higher, namely 1.35 V [50] and 1.14 V [34], respectively, reflecting better oxidation capacities for chlorite oxidation compared to HRP. For the couples Compound II/ferric enzyme the $E^{\circ\prime}$ values for MPO and LPO are 0.97 V [50] and 1.04 V [34], respectively, at pH 7. These values are slightly higher than the corresponding value for HRP being 0.93 V [12].

During one-electron oxidation of chlorite by Compound I/II chlorine dioxide has to be formed as a reaction product. This was demonstrated in the HRP-mediated transitions monitored by the increase of absorbance of ClO_2 at 359 nm. In the MPO/chlorite or LPO/chlorite systems ClO_2 could not accumulate since the reaction cycle is interrupted at the ferric state, which is immediately attacked by the excess of chlorite resulting in heme bleaching. Thus, neither HOCl (two-electron reduction product of chlorite) nor sufficient amounts of ClO_2 (one-electron oxidation product) could be formed which easily explains the absence of chlorination activity. We could also demonstrate that ClO_2 is unable to mediate heme degradation upon addition to ferric MPO.

Upon interaction with MPO chlorite destroys the structural integrity of MPO. Activity staining in SDS-PAGE, UV–vis- and EPR-spectroscopy clearly demonstrated that chlorite causes heme degradation, partly by release of free iron. Although the overall secondary composition of MPO was not affected as determined by far-UV ECD spectroscopy, the conformational and thermal stability was decreased and the light chain detached from the protein in SDS-PAGE under non-reducing conditions. This can easily be explained by the fact that in native MPO the prosthetic group (together with a Ca^{2+}-ion) crosslinks the light and heavy chains [51]. Upon degradation of the prosthetic group the two polypeptides fall apart under denaturing conditions.

Comparing effects of pure chlorite with the chlorite-containing drug Oxoferin, we observed nearly identical kinetics of its interaction with the relevant redox intermediates. Oxoferin also mediated heme bleaching. Thus, concerning the interaction with heme in MPO, chlorite is really an active compound in the OXO-K993-derived drug solution Oxoferin. To what extent the interaction of the chlorite-containing drugs Oxoferin and WF10 with MPO are responsible for the observed therapeutic effects of these drugs, remains unknown. As shown here, chlorite is able to inactivate MPO and LPO irreversibly with the ferric state representing the susceptible redox intermediate. Inactivation included heme degradation and iron release. Recently 2-thioxanthines were also described as potent irreversible inactivators of MPO [52,53]. However, kinetic analysis, mass spectrometry and X-ray crystal structures revealed that these inhibitors become oxidized by MPO and, finally, covalently attached to the heme prosthetic groups thereby blocking the entrance to the heme cavity. Being dependent on hydrogen peroxide 2-thioxanthines are typical mechanism-based inhibitors, whereas chlorite competes with H_2O_2 for binding to ferric MPO.

Data about potential chlorite actions under pathological conditions like cardiovascular diseases, where MPO is known for their adverse effects [54,55], are lacking. In therapeutic use, other possible chlorite effects are modulation and stimulation of immune responses [56], activation of macrophage functions [40], the stimulation of killer cell cytotoxicity [57], methemoglobin formation [44] and formation of chlorine dioxide. The later species has strong anti-microbial properties [58] and can be also derived from one-electron oxidation of chlorite by Compounds I and II of MPO or LPO. At inflammatory sites, the likelihood for the aforementioned chlorite activity might be increased considering enhanced levels of hydrogen peroxide at these sites. Taken together, chlorite can principally cause a number of divergent effects upon its application. Which effects under strong pathological conditions dominate needs to be further specified.

Abbreviations

MPO	human myeloperoxidase
LPO	bovine lactoperoxidase
HRP	horseradish peroxidase
MCD	monochlorodimedon
APF	aminophenyl fluorescein
CD	circular dichroism
DSC	differential scanning calorimetry

Acknowledgments

This project was supported by the Austrian Science Fund (FWF P25270-B22), by the German Federal Ministry of Education and Research (BMBF 1315883), and by the Sächsische Aufbaubank from a funding of the European Regional Development Fund (ERDF). S.H. was supported by the PhD program BioToP — Biomolecular Technology of Proteins (FWF W1224).

Appendix A. Supplementary data

Supplementary data to this article can be found online at http://dx.doi.org/10.1016/j.jinorgbio.2014.02.010.

References

[1] C.L. French, S.S. Yaun, L.A. Baldwin, D.A. Leonard, X.Q. Zhao, E.J. Calabrese, J. Appl. Toxicol. 15 (1995) 167–174.
[2] E.G. Hrycay, J.A. Gustafsson, M. Ingelman-Sundberg, L. Ernster, FEBS Lett. 56 (1975) 161–165.
[3] C.G. van Ginkel, G.B. Rikken, A.G. Kroon, S.W. Kengen, Arch. Microbiol. 166 (1996) 321–326.
[4] G. Mlynek, B. Sjoblom, J. Kostan, S. Fureder, F. Maixner, K. Gysel, P.G. Furtmuller, C. Obinger, M. Wagner, H. Daims, K. Djinovic-Carugo, J. Bacteriol. 193 (2011) 2408–2417.
[5] A.Q. Lee, B.R. Streit, M.J. Zdilla, M.M. Abu-Omar, J.L. DuBois, Proc. Natl. Acad. Sci. U. S. A. 105 (2008) 15654–15659.
[6] P. George, J. Biol. Chem. 201 (1953) 413–426.
[7] S. Shahangian, L.P. Hager, J. Biol. Chem. 256 (1981) 6034–6040.
[8] P.F. Hollenberg, T. Rand-Meir, L.P. Hager, J. Biol. Chem. 249 (1974) 5816–5825.
[9] W.D. Hewson, L.P. Hager, J. Biol. Chem. 254 (1979) 3182–3186.
[10] W.D. Hewson, L.P. Hager, J. Biol. Chem. 254 (1979) 3175–3181.
[11] S. Shahangian, L.P. Hager, J. Biol. Chem. 257 (1982) 11529–11533.
[12] C. Jakopitsch, H. Spalteholz, P.G. Furtmuller, J. Arnhold, C. Obinger, J. Inorg. Biochem. 102 (2008) 293–302.
[13] J. Arnhold, J. Flemmig, Arch. Biochem. Biophys. 500 (2010) 92–106.
[14] M.S. McGrath, J.O. Kahn, B.G. Herndier, Curr. Opin. Investig. Drugs 3 (2002) 365–373.
[15] R. Fenna, J. Zeng, C. Davey, Arch. Biochem. Biophys. 316 (1995) 653–656.
[16] P.G. Furtmuller, M. Zederbauer, W. Jantschko, J. Helm, M. Bogner, C. Jakopitsch, C. Obinger, Arch. Biochem. Biophys. 445 (2006) 199–213.
[17] L. Huang, G. Wojciechowski, P.R. Ortiz de Montellano, J. Biol. Chem. 281 (2006) 18983–18988.
[18] D.P. Nelson, L.A. Kiesow, Anal. Biochem. 49 (1972) 474–478.
[19] C.S. Furman, D.W. Margerum, Inorg. Chem. 37 (1998) 4321–4327.
[20] R. Floris, R. Wever, Eur. J. Biochem. 207 (1992) 697–702.
[21] P.G. Furtmuller, W. Jantschko, G. Regelsberger, C. Jakopitsch, N. Moguilevsky, C. Obinger, FEBS Lett. 503 (2001) 147–150.
[22] K.G. Paul, P.I. Ohlsson, in: K.M. Pruitt, J.O. Tenuovo (Eds.), The lactoperoxidase system, chemistry and biological significance, Marcel Dekker, New York, 1985, pp. 15–30.
[23] H.B. Dunford, Heme Peroxidases, Wiley VCH, New York, 1999.
[24] T. Chen, Anal. Chem. 39 (1967) 804–813.
[25] P.E. Thomas, D. Ryan, W. Levin, Anal. Biochem. 75 (1976) 168–176.
[26] L.P. Hager, D.R. Morris, F.S. Brown, H. Eberwein, J. Biol. Chem. 241 (1966) 1769–1777.
[27] J. Flemmig, J. Zschaler, J. Remmler, J. Arnhold, J. Biol. Chem. 287 (2012) 27913–27923.
[28] S. Stoll, A. Schweiger, J. Magn. Reson. 178 (2006) 42–55.
[29] B. Chance, Arch. Biochem. 21 (1949) 416–430.
[30] H. Hori, R.E. Fenna, S. Kimura, M. Ikeda-Saito, J. Biol. Chem. 269 (1994) 8388–8392.
[31] M. Zamocky, C. Jakopitsch, P.G. Furtmuller, C. Dunand, C. Obinger, Proteins 72 (2008) 589–605.
[32] B.G. Bolscher, R. Wever, Biochim. Biophys. Acta 788 (1984) 1–10.
[33] A.R. Bakkenist, J.E. de Boer, H. Plat, R. Wever, Biochim. Biophys. Acta 613 (1980) 337–348.
[34] P.G. Furtmuller, J. Arnhold, W. Jantschko, M. Zederbauer, C. Jakopitsch, C. Obinger, J. Inorg. Biochem. 99 (2005) 1220–1229.
[35] P.G. Furtmuller, U. Burner, W. Jantschko, G. Regelsberger, C. Obinger, Redox Rep. 5 (2000) 173–178.
[36] D. Maitra, F. Shaeib, I. Abdulhamid, R.M. Abdulridha, G.M. Saed, M.P. Diamond, S. Pennathur, H.M. Abu-Soud, Free Radic. Biol. Med. 63 (2013) 90–98.
[37] D.I. Pattison, M.J. Davies, Chem. Res. Toxicol. 14 (2001) 1453–1464.
[38] M.C. Hsu, R.W. Woody, J. Am. Chem. Soc. 93 (1971) 3515–3525.
[39] S.P. Raffanti, W. Schaffner, C.F. Federspiel, R.B. Blackwell, O.A. Ching, F.W. Kuhne, Infection 26 (1998) 202–207.
[40] V. Veerasarn, W. Boonnuch, C. Kakanaporn, Gynecol. Oncol. 100 (2006) 179–184.
[41] N. Yingsakmongkol, P. Maraprygsavan, P. Sukosit, J. Foot Ankle Surg. 50 (2011) 635–640.
[42] J. Hinz, H. Hautzinger, K.W. Stahl, Lancet 1 (1986) 825–828.
[43] M.S. McGrath, V. Kotelja, Pathobiology. 67 (1999) 277–281.
[44] E. Habermann, B. Muller, Klin. Wochenschr. 67 (1989) 20–25.
[45] Y. Hayashi, I. Yamazaki, J. Biol. Chem. 254 (1979) 9101–9106.
[46] I.R. Epstein, K. Kustin, J. Phys. Chem. 89 (1985) 2275–2282.
[47] J. Arnhold, P.G. Furtmuller, G. Regelsberger, C. Obinger, Eur. J. Biochem. 268 (2001) 5142–5148.
[48] I. Fabian, G. Gordon, Inorg. Chem. 30 (1991) 3785–3787.
[49] U.K. Kläning, K. Sehested, J. Holcman, J. Phys. Chem. 89 (1985) 760–763.
[50] P.G. Furtmuller, J. Arnhold, W. Jantschko, H. Pichler, C. Obinger, Biochem. Biophys. Res. Commun. 301 (2003) 551–557.
[51] T.J. Fiedler, C.A. Davey, R.E. Fenna, J. Biol. Chem. 275 (2000) 11964–11971.
[52] J. Ward, S.N. Spath, B. Pabst, P.A. Carpino, R.B. Ruggeri, G. Xing, A.E. Speers, B.F. Cravatt, K. Ahn, Biochemistry 52 (2013) 9187–9201.
[53] A.K. Tidén, T. Sjögren, M. Svensson, A. Bernlind, R. Senthilmohan, F. Auchère, H. Norman, P.O. Markgren, S. Gustavsson, S. Schmidt, S. Lundquist, L.V. Forbes, N.J. Magon, L.N. Paton, G.N. Jameson, H. Eriksson, A.J. Kettle, J. Biol. Chem. 286 (2011) 37578–37589.
[54] T.K. Rudolph, S. Wipper, B. Reiter, V. Rudolph, A. Coym, C. Detter, D. Lau, A. Klinke, K. Friedrichs, T. Rau, M. Pekarova, D. Russ, K. Knoll, M. Kolk, B. Schroeder, K. Wegscheider, H. Andresen, E. Schwedhelm, R. Boeger, H. Ehmke, S. Baldus, Eur. Heart J. 33 (2012) 1625–1634.
[55] C. Nussbaum, A. Klinke, M. Adam, S. Baldus, M. Sperandio, Antioxid. Redox Signal. 18 (2013) 692–713.
[56] T. Giese, M.S. McGrath, S. Stumm, H. Schempp, E. Elstner, S.C. Meuer, Cell. Immunol. 229 (2004) 149–158.
[57] L. Kuhne, M. Konstandin, Y. Samstag, S. Meuer, T. Giese, C. Watzl, J. Biomed. Biotechnol. (2011) 436587.
[58] C.J. Volk, R. Hofmann, C. Chauret, G.A. Gagnon, G. Ranger, R.C. Andrews, J. Environ. Eng. Sci. 1 (2002) 323–330.